Acta Materialia 233 (2022) 117970

Contents lists available at ScienceDirect

Acta Materialia

journal homepage: www.elsevier.com/locate/actamat

Zr diffusion in BCC refractory high entropy alloys: A case of 'non-sluggish' diffusion behavior

Jingfeng Zhang[a], Christian Gadelmeier[b], Sandipan Sen[a], Rui Wang[c], Xi Zhang[d], Yu Zhong[c], Uwe Glatzel[b], Blazej Grabowski[d], Gerhard Wilde[a], Sergiy V. Divinski[a,*]

[a] Institute of Materials Physics, University of Münster, Wilhelm-Klemm-Str. 10, Münster 48149, Germany
[b] Metals and Alloys, University of Bayreuth, Prof.-Rüdiger-Bormann-Str. 1, Bayreuth 95447, Germany
[c] Department of Mechanical Engineering, Worcester Polytechnic Institute, 100 Institute Rd, Worcester MA 01609, USA
[d] Institute for Materials Science, University of Stuttgart, Pfaffenwaldring. 55, Stuttgart 70569, Germany

ARTICLE INFO

Article history:
Received 2 November 2021
Revised 24 March 2022
Accepted 20 April 2022
Available online 29 April 2022

Keywords:
Diffusion
Refractory high-entropy alloy
HfNbTaTiZr
HfNbTiVZr
BCC crystalline lattice

ABSTRACT

Single phase (BCC solid solution) HfTiZrNbTa and HfTiZrNbV refractory high entropy alloys are synthesized and characterized. For the first time for BCC refractory high entropy alloys, tracer diffusion is measured using the short-living radioactive isotope ^{89}Zr in the temperature range of 1123 to 1423 K. A 'non-sluggish' diffusion behavior is clearly observed, highlighted by an enhancement of the measured diffusion rates with respect to the geometric mean of the diffusivities in the corresponding pure elements. The factors influencing self-diffusion in BCC multi-principal element alloys are discussed, including the chemical complexity, atomic size mismatch and the phonon broadening.

1. Introduction

The concept of high-entropy alloys (HEAs) was introduced in 2004 [1] and presents nowadays a focus of very intensive research. Due to the mixing of multiple principal elements which often form simple crystal structures, HEAs are expected to exhibit advanced physical and mechanical properties [1]. Four core effects were suggested to be inherent to HEAs: the high-entropy effect, sluggish diffusion, the cocktail effect, and severe lattice distortions [1,2]. We demonstrate here that sluggish diffusion is *not* an inherent HEA characteristic.

Among all the reported HEAs, refractory high entropy alloys (RHEAs) attract special attention because of their potential to be applied as high-temperature structural materials (up to 1600°C) [3]. Considering their outstanding strength in the temperature range from 1200 to 1600°C (e.g., MoNbTaW and MoNbTaVW RHEAs retain strengths of over 400 MPa at temperatures up to 1600°C [4]), RHEAs are expected to surpass superalloys as the materials of choice, e.g., for aerospace propulsion systems, land-based gas turbines, nuclear reactors, heat exchange tubing, or in the chemical processing industry [3,5]. RHEAs are based on refractory elements from group IV (Ti, Zr, and Hf), group V (V, Nb, and Ta), and group VI (Cr, Mo, and W). Showing a body centered cubic (BCC) structure, these alloys may contain secondary intermetallic phases like Laves or B2-ordered ones, especially for the non-equiatomic compositions [5].

RHEAs [6–9] and refractory alloys [10] in general are prone to the formation of non-protective oxides. Internal oxidation might be an issue, too, because the diffusion rate of oxygen through refractory metal oxides is fast enough to form a new oxide layer beneath the existing oxide scale. Moreover, a so-called 'pest' phenomenon is observed in some refractory alloys with Al or Si additions [6,11,12]. Despite the good oxidation resistance at low and high temperatures, these alloys fail catastrophically at intermediate temperatures by degradation to powder in oxidizing environments. It is a general consensus that such degradation results from preferential intergranular diffusion of a gaseous element, coupled with a temperature dependent hardening reaction [11]. Poor environmental resistance is one of the main factors inhibiting the development of RHEAs for high temperature structural applications [5].

Understanding diffusion behavior is not only of critical relevance for the oxidation resistance of RHEAs, but on quite general grounds in relation to phase stability and transformation kinetics in HEAs. Originally, the concept of 'sluggish diffusion' was proposed according to which self-diffusion slows down as the number of elements increases. Attractive enough, this idea [2] has stimulated a large number of investigations. In the most

* Corresponding author.
E-mail address: divin@uni-muenster.de (S.V. Divinski).

https://doi.org/10.1016/j.actamat.2022.117970
1359-6454/

widely studied FCC CoCrFeMnNi HEAs, chemical interdiffusion [2,13], tracer bulk diffusion [14–20], and even grain boundary diffusion [21,22] were systematically investigated. For BCC HEAs, there are some interdiffusion-related studies [23–27], and a single report on tracer diffusion of Co in the AlFeNiCoCuCr alloy [28], however, even the basic experimental tracer self-diffusion data in RHEAs were simply not measured so far. Therefore, it is extremely important to quantify the diffusion behavior in BCC HEAs through direct self-diffusion measurements. These measurements will contribute to verification and, if required, improvement of the CALPHAD-type mobility database MOBHEA2 [29]. Furthermore, new aspects with respect to common FCC systems might be seen as it was observed for HCP HEAs [30].

The single phase solid solution alloys TiZrHfNbTi and TiZrHfNbV, which were firstly reported in 2011 [31] and 2012 [32], respectively, are the most widely studied BCC RHEAs. TiZrHfNbTa, for example, reveals a high strength and good ductility at room temperature [31,31,33–47]. The lattice structure of TiZrHfNbTa RHEA was assumed to be single-phase BCC down to room temperature. Recent studies, however, show that two BCC phases (one is (Nb+Ta)-rich and another is (Hf+Zr)-rich) are formed after severe cold work and annealing at 700 – 900°C, or that even a (Hf+Zr)-rich HCP phase can be obtained after severe plastic deformation followed by annealing at 300°C or 500°C [35,40]. These results indicate that slow self-diffusion may play an important role in producing a variety of kinetically stable microstructures in RHEAs. The TiZrHfNbV RHEA has high strength, good ductility at room temperature, and a relatively low density as compared to the TiZrHfNbTa RHEA [32,48,49].

Furthermore, plenty of research concerning high entropy superhard nitride layers was conducted [32,50–52]. These studies reveal that the formation of interfaces in multicomponent coatings and the formation of the stress states of nanocrystals are affected by thermally-activated diffusion of small atoms like nitrogen and oxygen.

For all these reasons, the present study is focused on self-diffusion of Zr in TiZrHfNbTa and TiZrHfNbV, the two representative RHEAs with the same BCC lattice structure, mixing entropy, and similar compositions. Based on the obtained diffusion coefficients, the concept of 'sluggish' diffusion is falsified for these systems. The focus on Zr diffusion was dictated by the availability of the suitable ^{89}Zr radioisotope.

2. Experimental details

2.1. Manufacturing of the alloys

For the production of the TiZrHfNbTa and TiZrHfNbV RHEAs, pure elements (purity of 99.99%) were used in form of granules with sizes between 2 and 5 mm. Before melting, the granules were cleaned with ethanol in an ultrasonic bath station. The alloys were melted under argon atmosphere on a water-cooled copper chill plate in an arc melting furnace [53]. Due to the high melting temperatures (more than 2000°C for TiZrHfNbTa [54] and around 1590°C for TiZrHfNbV [49]), only relatively small quantities were produced to achieve the best chemical homogeneity. Each alloy was pre-melted in several small buttons of 25 g in weight by using a current of 750 A. After flipping the buttons 8 times, several buttons were melted to form long rods with lengths of around 100 mm and diameters of 6.5 mm and 12 mm for TiZrHfNbTa and TiZrHfNbV RHEAs, respectively.

2.2. Alloy characterization

The rods were cut into several segments of about 25 mm in length and were cleaned in ethanol in an ultrasonic bath station. After annealing at 1200°C for 48 h in a high-temperature furnace under vacuum using quartz ampoules, the samples were quenched in cold water to room temperature, at an estimated cooling rate of about 10 K/s.

The chemical composition was checked by using micro-X-ray fluorescence analysis (μ-XRF, Orbis PC; Ametek) on several cross sections of different segments to confirm the equiatomic composition of both high entropy alloys. Two pieces of TiZrHfNbTa and TiZrHfNbV were analyzed by X-ray diffraction (XRD) (Siemens D5000, Cu-K_α radiation) and a scanning electron microscope (SEM) equipped with energy dispersive spectroscopy (EDS) to determine the phase structure and compositional homogeneity of the alloys.

Electron back-scatter diffraction (EBSD) measurements of both alloys were conducted using a Zeiss Sigma 300 VP and a Hikari Plus EBSD camera to check the grain size and preferred orientations.

Table 1
Annealing temperatures T, times t, and the determined diffusion coefficients D for ^{89}Zr in the TiZrHfNbTa and TiZrHfNbV RHEAs. The typical experimental uncertainties of the D values are estimated to be less than about 20%.

Alloy	T (K)	t (10^3 s)	D (m^2/s)
TiZrHfNbTa	1123	923.4	4.22×10^{-16}
	1173	252	6.10×10^{-16}
	1223	172.8	1.71×10^{-15}
	1273	57.6	3.84×10^{-15}
	1348	14.4	6.45×10^{-15}
	1423	5.4	1.96×10^{-14}
TiZrHfNbV	1223	172.8	9.55×10^{-15}
	1273	57.6	1.63×10^{-14}
	1323	43.2	1.84×10^{-14}
	1348	14.4	2.86×10^{-14}
	1423	5.4	6.59×10^{-14}

2.3. Tracer diffusion measurements

Samples were cut into 1.5 mm thick discs with diameters of 6.5 mm and 12 mm for TiZrHfNbTa and TiZrHfNbV, respectively, using a spark erosion method. All discs were then pre-annealed to reduce mechanical stresses and achieve equilibrium defect concentrations at the intended diffusion temperatures. The annealing treatments were performed in evacuated quartz tubes filled with purified (5N) Ar.

The ^{89}Zr radioisotope (half-life of 3.3 days) was provided by PerkinElmer LAS GmbH, Germany. The original oxalic acid-based solution was highly diluted using double-distilled water and was then deposited on a mirror-like surface of the disc-shaped samples and left for drying. Diffusion annealing treatments were carried out in sealed quartz tubes under purified (5N) Ar atmosphere. Annealing times and temperatures are listed in Table 1. The furnace temperature was controlled within ±1 K using a certified Ni/NiCr thermocouple (type K).

After annealing, the penetration profiles were determined using serial sectioning via high-precision parallel grinding. The sections of 0.3 to 10 μm thickness were ground. The section thickness was determined with a relative accuracy better than ±0.03% by weighing the samples before and after grinding on a microbalance. The intensity of the γ-decays (the energy of the main line of 908.97 keV) was determined by a solid Ge-detector equipped with a multi-channel 16K energy discriminator. A proper counting time correction for the isotope decay has been applied and the statistical uncertainty of the measurements was estimated to be less than 2% in all relevant energy windows.

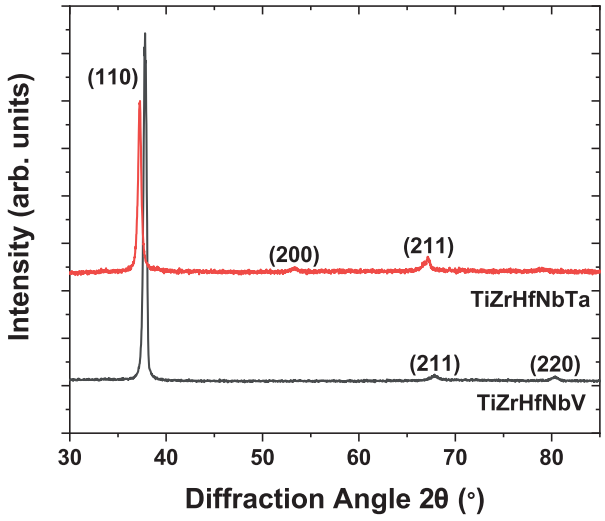

Fig. 1. X-ray diffraction patterns of the TiZrHfNbTa and TiZrHfNbV HEAs. Peaks corresponding to the crystallographic planes of the BCC phase are indicated.

3. Results

3.1. Microstructure and chemical homogeneity

The alloy compositions were measured with μ−XRF and obtained as $Ti_{17.9}Zr_{20.1}Nb_{22.0}Hf_{20.3}Ta_{19.7}$ and $Ti_{19.7}Zr_{19.9}Nb_{20.7}Hf_{19.2}V_{20.5}$ (in at.%). The XRD patterns are presented in Fig. 1 and they substantiate the single phase BCC structures of both, TiZrHfNbTa and TiZrHfNbV. Indexing the XRD spectra, the lattice parameters were determined as 0.3374 and 0.3403 nm for TiZrHfNbTa and TiZrHfNbV, respectively.

As an example, Fig. 2b shows the result of EBSD measurements of the TiZrHfNbV HEA samples. The EBSD grain orientation map of the TiZrHfNbTa RHEA from a previous publication [53] can be seen in Fig. 2a. In both cases, grains with an average size of more than 100 μm and no particular texture are observed. The EDS analysis shown in Fig. 3a and c confirms the homogeneous elemental distribution of the two RHEAs after the homogenization annealing.

The equilibrium diagrams of TiZrHfNbTa and TiZrHfNbV were calculated by Thermo-Calc [55] with the TCHEA4 database, see Fig. 4. The BCC solid solution of TiZrHfNbTa decomposes into two disordered BCC phases below about 1300 K and a further HCP phase appears at $T < 1000$ K, Fig. 4a. Since the present diffusion measurements have been carried out in the temperature range of 1123–1423 K, the appearance of a second BCC phase has to be expected at equilibrium conditions, though it could be hindered kinetically. We performed a detailed SEM and EDS characterization of the samples annealed at identical (temperature and time) conditions as used for the diffusion studies. No indication of a second phase was observed at any of the investigated conditions. In Fig. 3b, the microstructure and the element distributions after annealing at 1123 K for 2 days are shown as an example. Although previous studies on TiZrHfNbTa RHEAs reported the formation of new BCC phases at similar temperatures, these studies examined severely deformed [35] or nanocrystalline [40] alloys and the phase decomposition was observed dominantly at grain boundaries. The present study on a coarse-grained (equiaxed) TiZrHfNbTa RHEA substantiates that the kinetics of the phase decomposition is retarded at least on the time scale relevant for the present diffusion experiments.

As for the TiZrHfNbV RHEA, we also checked the phase stability using SEM and EDS analyses. In accordance to the phase fraction calculations, Fig. 4b, we observed only one single disordered BCC phase in the temperature interval of 1273–1473 K. A strong segregation of vanadium to grain boundaries was found after annealing treatment below 1323 K. The most significant segregation was induced by annealing at 1173 K for 3 days, Fig. 3d. However, the grain boundary segregation does not affect the volume diffusion measurements, though it has to be taken into account when analysing the grain boundary diffusion contribution. V has the smallest atomic radius of all alloying elements, which may be responsible for the strong segregation tendency of V. Following McLean's reasonings [56], the elastic contributions dominate the segregation energy of a solute. Further research on vanadium segregation at grain boundaries would be important for the study of the phase stability in the TiZrHfNbV RHEA, although it is beyond the scope of the present study.

In the present context, the most important conclusion is that the V grain boundary segregation does not affect the volume diffusion data. According to exact solution of the grain boundary diffusion problem [57], the tracer concentration at depths below about $2\sqrt{Dt}$ is dominated by direct volume diffusion from the sample surface (here D is the volume diffusion coefficient−the Zr self-diffusion coefficient in our case−and t is the diffusion time). The total amount of V atoms segregated at grain boundaries is negligibly small and does not affect strongly the alloy composition in the present case in view of the large grain size, i.e., because of a small total volume fraction of the grain boundary-related material (which can be estimated to be less than 10^{-5} assuming a grain boundary width of about 1 nm) and a relatively small grain boundary excess of V atoms.

3.2. Diffusion coefficients

As an example, the concentration profiles of Zr diffusion in the TiZrHfNbTa and TiZrHfNbV RHEAs measured at 1423 K are shown in Fig. 5. Other penetration profiles are of a similarly high quality.

In the case of TiZrHfNbTa, two contributions can clearly be distinguished, Fig. 5. The first, near surface contribution is related to volume diffusion, whereas the deeper contribution represents grain boundary diffusion.

The instantaneous source (Gaussian) solution of the bulk tracer diffusion problem is found to be appropriate under the present conditions, Fig. 5, and the corresponding branches of the concentration profiles were approximated as

$$C(x,t) = \frac{M}{\sqrt{\pi Dt}} \exp\left(-\frac{x^2}{4Dt}\right). \quad (1)$$

Here $C(x,t)$ is the concentration of the tracer atoms at the depth x from the surface after the time t and M is the initial tracer amount.

A further, short-circuit diffusion contribution was observed in some cases, as it is shown in Fig. 5 for Zr diffusion in TiZrHfNbTa, and it is associated with grain boundary diffusion. It should be noted here that not all samples were ground to the depths where grain boundary diffusion could be clearly seen during the high-precision parallel grinding process. Such handling of the samples was dictated by the very short half-life of the ^{89}Zr radioisotope. The corresponding tracer distribution is analysed in the framework of the so-called B-type kinetic regime of grain boundary diffusion after Harrison's classification [58] using Le Clair's functional form [59],

$$C(x,t) = C_0 \exp\left(-Ax^{6/5}\right), \quad (2)$$

where C_0 and A are constants [57]. We have to highlight that the present study is focused on volume diffusion and reliable measurements of the grain boundary diffusion contribution were hindered by the short half-life of ^{89}Zr. Therefore, a combination of Eqs. (1) and (2) was used to approximate the measured concen-

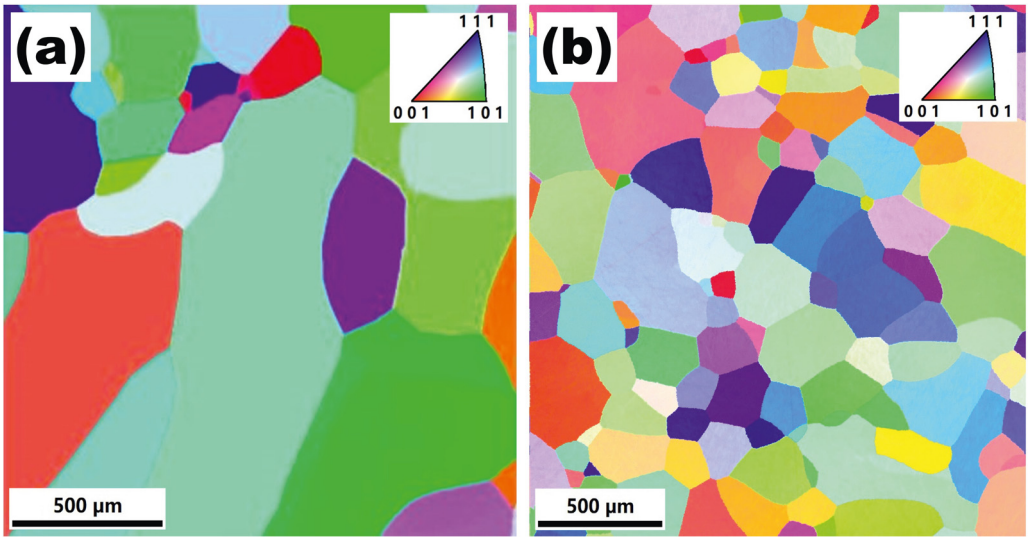

Fig. 2. EBSD grain orientation map of the (a) TiZrHfNbTa and (b) TiZrHfNbV RHEAs. The grain colors correspond to the orientations of the crystallographic planes with respect to the upward direction (the stereographic triangle is shown in the inset). Note that the EBSD map for TiZrHfNbTa in (a) represents a zoom-in view of a larger area presented in our previous work by Taheriniya et al. [53].

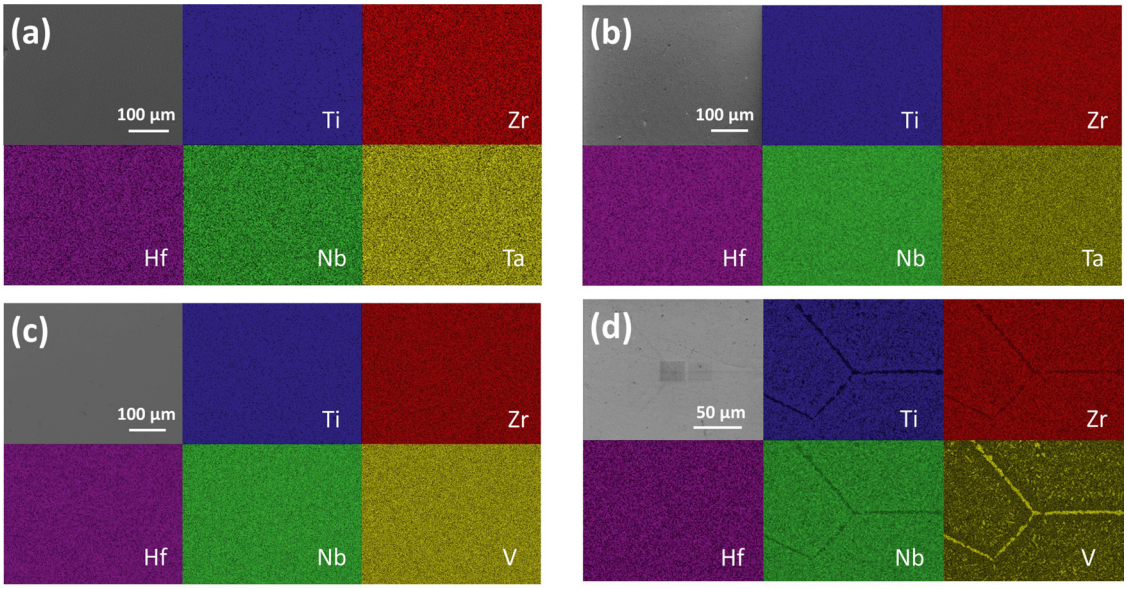

Fig. 3. SEM photographs and representative elemental EDS maps of TiZrHfNbTa annealed (a) at 1423 K for 7 days and (b) at 1123 K for 2 days, as well as TiZrHfNbV annealed (c) at 1423 K for 7 days and (d) at 1173 K for 3 days. The scale bar applies to all images within each sub-figure.

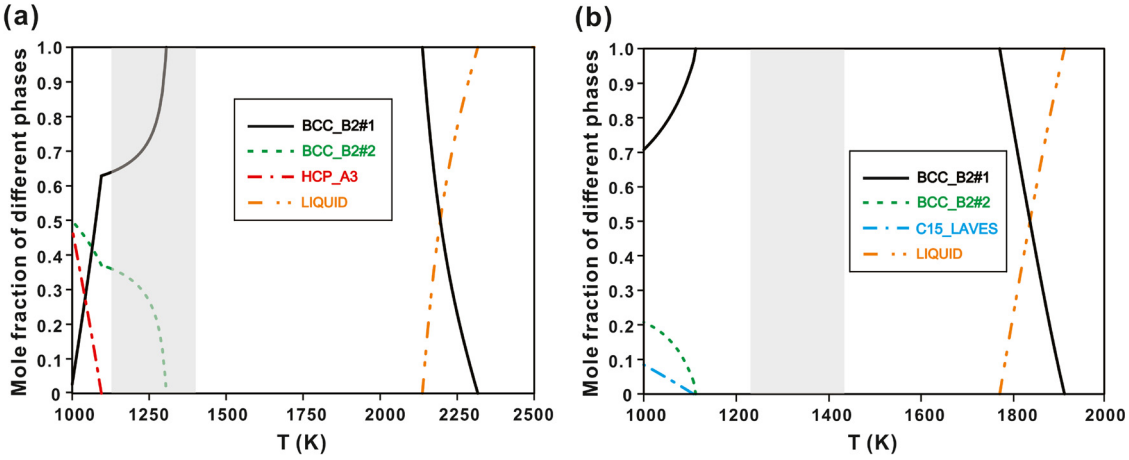

Fig. 4. Equilibrium diagrams of (a) TiZrHfNbTa and (b) TiZrHfNbV calculated with Thermo-Calc [55] utilizing the TCHEA4 database. The light gray boxes indicate the temperature ranges of the present diffusion annealing treatments.

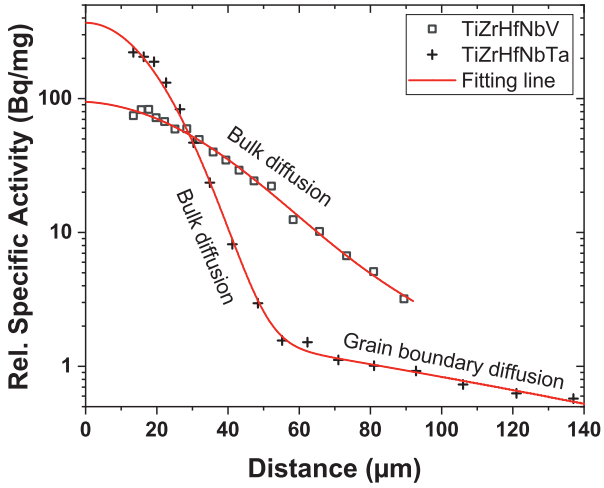

Fig. 5. Concentration profiles of Zr tracer diffusion measured at 1423 K in the TiZrHfNbTa and TiZrHfNbV RHEAs. The solid lines represent fits according to simultaneous bulk and (if present) grain boundary diffusion, Eqs. (1) and (2).

tration profile and determine reliably the volume diffusion coefficients, D, see red lines in Fig. 5.

The determined volume diffusion coefficients are reported in Table 1 together with the experimental conditions for the two RHEAs under investigation. In a single measurement, the estimated uncertainty of the determined tracer diffusion coefficients is below 20%.

The diffusion coefficients of Zr are found to follow an Arrhenius-type temperature dependence (in m^2/s),

$$D = \left(4.77^{+21}_{-3.9}\right) \cdot 10^{-9} \exp\left(-\frac{(134.2 \pm 18)\,\mathrm{kJ/mol}}{RT}\right) \quad (3)$$

for TiZrHfNbV and

$$D = \left(3.77^{+16}_{-3.1}\right) \cdot 10^{-8} \exp\left(-\frac{(172.4 \pm 11)\,\mathrm{kJ/mol}}{RT}\right) \quad (4)$$

for TiZrHfNbTa. Here RT has its usual meaning.

4. Discussion

4.1. Diffusion in the TiZrHfNbV and TiZrHfNbTa RHEAs

The experimentally determined tracer diffusion coefficients in the TiZrHfNbV and TiZrHfNbTa HEAs are shown in Fig. 6a and b as a function of the inverse absolute temperature, T^{-1}, and the inverse homologous temperature, T_m/T, respectively. Here T_m is the melting point of the corresponding alloys. The melting points of TiZrHfNbTa (2317 K) and TiZrHfNbV (1914 K) RHEAs were estimated using Thermo-Calc [55] with the TCHEA4 database, as shown in Fig. 4. The calculated melting point of TiZrHfNbV is quite close to the experimentally measured melting point (1863 ± 20 K), which was determined by an IRCON high-temperature ratio pyrometer in a high-frequency induction furnace [49]. The accuracy of the phase transition simulation of TiZrHfNbTa through the TCHEA4 database has also been confirmed by experiments [35,40].

At the same absolute temperatures, the diffusion rates in TiZrHfNbV are found to be faster than those in TiZrHfNbTa, Fig. 6a. The activation energy of Zr diffusion in the TiZrHfNbTa HEA is somewhat higher, which correlates with its higher melting point. The pre-exponential factor, D_0, of Zr diffusion in TiZrHfNbTa HEA is larger, too.

The pre-exponential factor D_0 is usually expressed as [60]:

$$D_0 = g f a^2 \nu_0 \exp\left(\frac{\Delta S}{R}\right), \quad (5)$$

where g is a geometric factor (= 1 for cubic lattices), f is the correlation factor, a is the lattice parameter, ν_0 is the attempt frequency (often approximated by the Debye frequency), and ΔS is the diffusion entropy. For a vacancy-mediated diffusion mechanism, the correlation factor arises due to an increased probability of reversed atomic jumps that result in reduced diffusion distances with respect to those for a completely random atom movement [60]. The diffusion entropy is the change of the entropy of lattice vibrations originating from a constrained movement of the diffusing atom through a saddle point configuration [60]. In this study, g, a, and ν_0 of these two RHEAs are exactly the same or very similar. The difference in D_0 is mainly due to the difference of the diffusion entropy ΔS and to a minor extent due to the difference of the correlation factor f. In a multi-component alloy, the atomic correlation factors f are temperature dependent (even the vacancy correlation factor is less than unity) and their values can be assessed via Kinetic Monte Carlo (KMC) simulations [61], which appeals for a further research on diffusion entropy and its influencing factors.

Zr diffuses faster in TiZrHfNbV with respect to that in TiZrHfNbTa if the diffusion coefficients are compared on the absolute temperature scale, Fig. 6a. An opposite relation holds when the tracer diffusion rates are compared on the homologous temperatures scale, Fig. 6b. The difference in the melting points (the melting point of TiZrHfNbV is lower) is the reason of this behavior, since the diffusion measurements in TiZrHfNbV are performed at higher homologous temperatures. It should be mentioned that both TiZrHfNbTa and TiZrHfNbV show quite low melting points compared to the average melting points of the alloying elements. The melting point of the TiZrHfNbV is even lower than that of Ti (1941 K), which has the lowest melting point of all the alloying elements.

4.2. Diffusion in refractory HEAs and other BCC matrices

The concept of 'sluggish diffusion' has been studied in several HEA alloying systems, especially in CoCrFeMnNi HEA [2,16–20,22,30]. Recent results from these studies indicate that the diffusion behavior in these HEAs is quite complex and should not be considered as 'sluggish' and the effect of chemical complexity is quite limited among all the factors that influence diffusion.

In order to analyse further the influence of the large number of alloying elements, corresponding to an enhanced configurational (mixing) entropy, on diffusion in these two refractory HEAs, a comparison with the literature data on tracer diffusion of Zr in various relevant BCC refractory metals and alloys is given in Figs. 6 and 7, including the BCC pure elements Ti, Zr, Nb, and V [62–64] (Fig. 6), as well as BCC binary systems Zr–51%Ti [65], Zr–5%Nb, Zr–16%Nb, Zr–28%Nb [66], Hf–10%Nb and Hf–18%Nb [67] (Fig. 7).

In Fig. 6a, Zr tracer diffusion in BCC pure elements Ti, Zr, Nb, and V is shown against the inverse absolute temperature and a strong correlation of Zr diffusion rates in pure BCC refractory elements with the melting points of the corresponding metals is seen. The Zr diffusivities follow the order $D_{Ti} > D_{Zr} > D_V > D_{Nb}$, which is consistent with the relation between the melting points of these elements. The higher activation energies of Zr diffusion in V and Nb are also visible by comparing the corresponding slopes. Figure 7a shows Zr tracer diffusion in binary systems Zr–51%Ti, Zr–5%Nb, Zr–16%Nb, Zr–28%Nb, Hf–10%Nb and Hf–18%Nb against the inverse absolute temperature. In the binary alloys, Zr diffuses faster when it is alloyed with a lower melting point element, Ti,

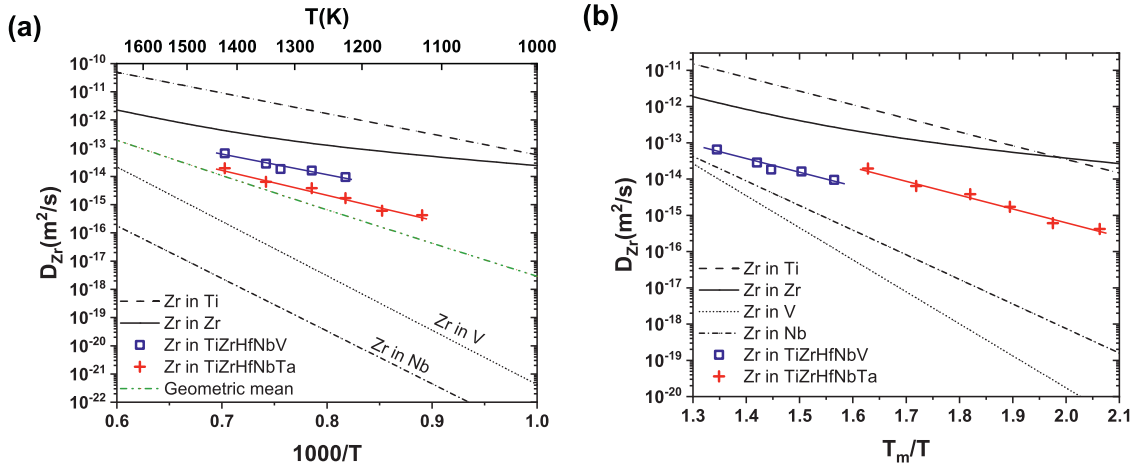

Fig. 6. Zr diffusion coefficients, D_{Zr}, in the two investigated RHEAs compared to Zr diffusion coefficients in the BCC phases of the respective pure metals (Ti, Zr, Nb, and V) as a function of the inverse absolute, T^{-1}, (a) and the inverse homologous, T_m/T, (b) temperature. In (a), the geometric mean of the diffusion coefficients in pure elements is shown for comparison (diffusion in pure Hf was replaced by that in Hf–10%Nb).

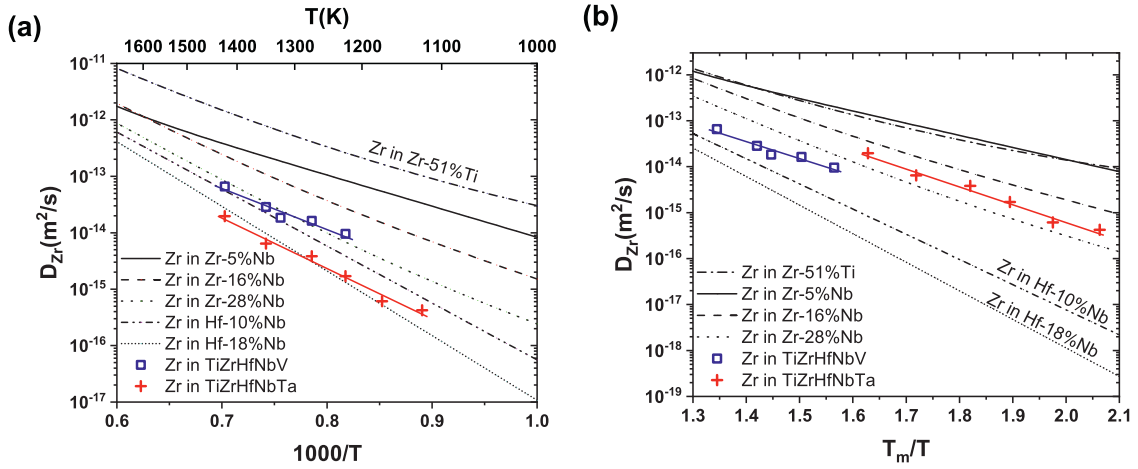

Fig. 7. Zr diffusion coefficients, D_{Zr}, in the two investigated RHEAs compared to Zr diffusion coefficients in various relevant BCC binary subsystems Zr–5%Nb, Zr–16%Nb, Zr–28%Nb, Zr–51%Ti, Hf–10%Ni and Hf–18%Nb (in at.%) as a function of the inverse absolute, T^{-1}, (a) and the inverse homologous, T_m/T, temperature.

while the opposite is seen when it is alloyed with a higher melting point element, Nb. The diffusivity decreases when the composition of Nb increases. The diffusion coefficients of Zr in TiZrHfNbV and TiZrHfNbTa HEAs lie between the data for pure Ti and V, which seems to be predictable. However, taking into account that diffusion of Zr in Ta and Hf, the two metals with very high melting points, is very likely to be slow (not measured so far), one may hypothesize that Zr diffusion in the two RHEAs seems to be even enhanced rather than retarded with respect to an 'averaged' behavior when compared using an inverse absolute temperature scale (see also below).

On the homologous temperature scale, the general trends for Zr diffusion in these BCC matrices are quite clear, Figs. 6b and 7b. The Arrhenius lines of Zr diffusion in group V elements (V and Nb) are closer than before, which can also be found for group IV elements (Ti and Zr). Conspicuously, retarded diffusion in the TiZrHfNbV can be found, while diffusion in the TiZrHfNbTa is somewhat enhanced. It's unexpected to observe opposite diffusion behaviors for the two very similar RHEAs with the same lattice structure and configurational entropy, as well as similar lattice parameters and compositions. Subsequently, several physical properties will be analyzed for their influence on the diffusion rate in these alloying systems.

4.2.1. Mixing entropy

The ideal mixing entropies, ΔS_{mix}, can be straightforwardly shown to follow the order

$$\begin{aligned}\Delta S_{mix}^{TiZrHfNbTa} &= \Delta S_{mix}^{TiZrHfNbV} \\ &> \Delta S_{mix}^{Zr-51\%Ti} > \Delta S_{mix}^{Zr-28\%Nb} > \Delta S_{mix}^{Hf-18\%Nb} \\ &> \Delta S_{mix}^{Zr-16\%Nb} > \Delta S_{mix}^{Hf-10\%Nb} > \Delta S_{mix}^{Zr-5\%Nb}. \end{aligned} \quad (6)$$

However, no straightforward correlation between the variation of the diffusivities and those of the mixing (configurational) entropy was found. Therefore, the influence of high configurational entropy on the diffusion is not straightforward, and we must conclude that the effect of the specific alloying elements dominates the diffusion behavior.

4.2.2. Potential energy fluctuation

The potential energy fluctuations in the potential energy landscape of the lattice sites are considered to contribute towards the creation of highly stable low energy sites, which can act as atomic traps and result in sluggish diffusion [2]. It was proposed [68] that the potential energy fluctuations, x_p, can be decomposed into a sum of elastic and chemical contributions, $x_p = x_e + x_{ch}$. According to He et al. [68], the normalized potential energy fluctuations due

to the atom size misfit, x_e, can be expressed as follows,

$$x_e = 4.12\delta \times \sqrt{\frac{\bar{K}\bar{V}}{k_B T}}, \tag{7}$$

where $\bar{K}$ is the average bulk modulus, $\bar{V}$ the average atomic volume. The lattice mismatch δ is,

$$\delta = \sqrt{\sum_{i=1}^{n} X_i \left(1 - \frac{r_i}{\sum_i X_i r_i}\right)^2}, \tag{8}$$

where X_i is the composition (mole fraction) of the constituent element i and r_i is its atomic radius.

The normalized potential energy fluctuations due to the chemical bond misfit, x_{ch}, are

$$x_{ch} = 2\sqrt{\frac{\sqrt{\sum_i \sum_{j,i\neq j} X_i X_j \left(H_{ij} - \bar{H}\right)^2}}{k_B T}}, \tag{9}$$

where H_{ij} denotes the mixing enthalpy between the i'th and j'th element and $\bar{H}$ the average of H_{ij}. The binary mixing enthalpy can be estimated by Miedemas macroscopic model [69]. This approach has been utilized for analysing diffusion behavior in FCC high-entropy alloys [70].

The potential energy fluctuations follow the order $x_{Zr-16\%Nb} > x_{Zr-5\%Nb} > x_{Zr-28\%Nb} > x_{Zr-51\%Ti} > x_{TiZrHfNbTa} > x_{TiZrHfNbV}$ at 1273 K, and there is no obvious correlation between the potential energy fluctuations and the diffusion coefficients. It should be added that in the quantification of the potential energy fluctuations we may also use Thermo-Calc with the TCHEA4 database instead of Miedema's model to estimate the mixing enthalpies. The calculation results would be somewhat different, but the final conclusion is not affected.

4.2.3. Lattice mismatch

Recently, vacancy-assisted diffusion in 57 random, equimolar alloys that formed from Cu, Ag, Au, Ni, Pd, and Pt based on the well-tested embedded atom method was examined by Daw and Chandross [71] They concluded that simply increasing the number of constituents in FCC high entropy alloys does not systematically alter diffusion. In fact, the lattice mismatch, δ, Eq. (8), was concluded to play a dominant role: sluggish diffusion is more likely to occur in a window of small lattice mismatch (1–3%), while a larger number of alloys (with $\delta > 3\%$) exhibits significantly faster diffusion. After Daw and Chandross [71], *vacancy* diffusion in a compound is enhanced with respect to the geometric mean of the corresponding values in pure elements by a factor of (in author's notations)

$$\frac{D^v}{\langle D^v \rangle} = \exp\left(-7.14\delta + 901.8\delta^2\right), \tag{10}$$

where D^v is the vacancy diffusion coefficient in an n-component equiatomic alloy and $\langle D^v \rangle = \left(\prod_{i=1}^{n} D_i^v\right)^{1/n}$ is the geometric mean of the vacancy diffusion coefficients in the pure elements.

In the case of the FCC CoCrFeMnNi alloy with a relatively low lattice distortion of about 1.7%, this factor is about unity, ≈ 1.1. The lattice distortions δ for the two RHEAs TiZrHfNbTa and TiZrHfNbV studied in this work are equal to 3.8% and 5.9%, respectively. Then, the enhancement factors, $D^v/\langle D^v \rangle$, are predicted to about 3 and 15, respectively.

Here, we may test the predictions, Eq. (10), adopting them to *tracer diffusion of a selected element*, i.e. Zr, in an equiatomic RHEA. It is obvious that the vacancy diffusion coefficients (experimentally non-measurable quantities) and the tracer diffusion coefficients of a given element i (the measurable quantities) are related by the value of the corresponding correlation factors, f_i, which are temperature-dependent [60].

In Fig. 6a, a hypothetical Zr diffusivity in the TiZrHfNbV alloy as an 'averaged' diffusivity of Zr in all constituting elements is plotted. An enhancement of the Zr diffusion rates with respect to this hypothetical averaged behavior is obvious and the enhancement depends strongly on temperature, being about 5 at 1450 K and approaching a value of about 20 at $T = 1200$ K. In the estimations, the diffusion rates of Zr in a Hf–10%Nb alloy [67] were used, since to the best of our knowledge Zr diffusion in pure Hf is not measured so far. This comparison is not completely suitable for the TiZrHfNbTa RHEA, because the tracer diffusion coefficients of Zr in pure Ta have not been measured yet. It should be noted that we used the experimentally determined lattice parameters instead of the average lattice parameters, however the difference is small and does not affect the conclusion.

From the above comparison, we conclude that, at least in the two BCC refractory high-entropy alloying systems studied in this work, the chemical complexity such as the mixing enthalpy or the potential energy fluctuation does not induce sluggish tracer diffusion. Furthermore, there is no correlation between these parameters and the Zr diffusion rates. The hypothesis of lattice mismatch seems to be more applicable to the present BCC systems and the Zr diffusivity is *enhanced* with respect to the anticipated averaged behavior. The enhancement is strongly temperature-dependent, which cannot be predicted by Eq. (10).

4.3. Absence of non-Arrhenius diffusion in BCC RHEAs

A prominent non-linearity of the temperature dependence of tracer diffusion in some BCC phases is seen in the Arrhenius coordinates [66], cf. Figs. 6 and 7. In the case of the β (BCC) phases of Ti, Zr, and Hf, which undergo a $\beta \rightarrow \alpha$ (HCP) transition, the curvature has been explained by pronounced softening of the (111) phonon modes [72–74] which enhances the vibrational entropy contribution to vacancy-mediated diffusion. Alloying of pure Zr by the β-stabilizer Nb reduces both phonon softening and the diffusion anomaly [66].

Generally, the diffusion anomaly, i.e., non-Arrhenius behaviour, can be attributed to the presence of either (a) different diffusion mechanisms or (b) a temperature-dependent thermal activation (i.e. formation and migration free energies), where the latter was shown to be the most probable case [66]. As a result, according to Eq. (3), any non-linearity in the temperature-dependent activation energy Q may introduce a curvature into the Arrhenius plots. Within the experimental temperature range, the main contributions to the temperature dependence of Q in the vacancy mechanism are expected to be the vacancy formation and migration entropies due to thermal vibrations, i.e., contributions from phonons. Previous *ab initio* calculations of vacancy formation Gibbs energies of Al, Cu [75] and Ni [76], reveal strong non-linearity of the temperature dependence of the vacancy formation entropy. Reasonable agreement with experiments can only be achieved when explicit anharmonic vibrations are taken into account, highlighting the importance of the anharmonicity in the vacancy energetics at elevated temperatures. Theoretical investigations of the full temperature-dependent vacancy migration entropy including anharmonicity, however, have not yet been reported due to technical challenges and the considerable computational effort [77].

The present data on the five-component RHEAs provide no indications of a non-linearity of Zr tracer diffusion in the investigated temperature intervals, Figs. 6 and 7. Recently, the impact of chemical complexity on phonons in bcc RHEAs has been investigated via density-functional-theory-informed finite temperature calculations of vibrational entropy contributions [78,79]. An increase of the force constants by alloying with Nb or Ta has been predicted [78] that correlates with the absence (in the temperature interval under investigation) of a diffusion anomaly for RHEAs in compar-

ison with the β-phases of Ti, Hf or Zr. Despite these findings, the phonon behavior and their contributions to the vibrational entropy with the presence of vacancies—critical knowledge to understand diffusion in HEAs—are still missing, which calls for future studies with new methodological developments. Note that, besides the non-linearity introduced by phonons, *ab initio* studies of vacancies in binary Cu-Ni [80] and HCP HEAs [81] showed that 'configurational excitations' of various local chemical environments may also provide a non-negligible negative excess entropy of vacancy formation, resulting in non-Arrhenius behavior. The competition and/or the coupling effect between the vibrational excitation and the configurational excitation may also play a role concerning the diffusion anomaly.

5. Conclusions

TiZrHfNbTa and TiZrHfNbV BCC refractory high entropy alloys were produced and characterized using XRD, SEM, including EBSD and EDS analyses.

For the first time, volume diffusion of a selected element was measured in BCC RHEAs utilizing the relatively short-living radioactive isotope ^{89}Zr. The main results are summarized as follows:

- The temperature dependencies of Zr tracer diffusion in both RHEAs follow linear Arrhenius-type behaviors (in the temperature intervals investigated). A larger activation enthalpy, Q, governs mainly the slower diffusion rates of Zr in TiZrHfNbTa, while the relatively lower melting point is responsible for slower diffusion in TiZrHfNbV when analyzed as a function of the inverse homologous temperature.
- Tracer diffusion of Zr in BCC RHEAs is obviously non-sluggish when compared with other BCC matrices, considering both the absolute or homologous temperature scales. Zr diffusion rates in these RHEAs are roughly similar to those in a binary Zr–28%Nb alloy when considered on the homologous temperature scale and the chemical complexity of the five-component HEA does not retard diffusion further.
- Lattice distortions are found to contribute to an enhancement of Zr diffusivity with respect to the anticipated 'averaged' behavior which may be predicted analysing the diffusion rates in pure elements.

Declaration of Competing Interest

The authors declare that they have no known competing financial interests or personal relationships that could have appeared to influence the work reported in this paper.

Acknowledgement

The authors wish to thank Dr. G. Mohan Muralikrishna, Dr. Hongbo Zhou, Haihong Jiang, Baixue Bian and Manoel W. Da Silva Pinto (Institute of Materials Physics, University of Münster, Germany) for the help with measurements. Jingfeng Zhang is grateful to the China Scholarship Council (CSC) for its financial support. Financial support from the German Science Foundation (DFG) via research grants DI 1419/13-2, DI 1419/17-1, GR 3716/5-1, and WI 1899/32-2 within the priority program SPP2006 'Compositionally Complex AlloysHigh Entropy Alloys (CCA-HEA)' is acknowledged.

References

[1] J.W. Yeh, S.K. Chen, S.J. Lin, J.Y. Gan, T.S. Chin, T.T. Shun, C.H. Tsau, S.Y. Chang, Nanostructured highentropy alloys with multiple principal elements: novel alloy design concepts and outcomes, Adv. Eng. Mater. 6 (5) (2004) 299–303.
[2] K.-Y. Tsai, M.-H. Tsai, J.W. Yeh, Sluggish diffusion in Co-Cr-Fe-Mn-Ni high-entropy alloys, Acta Mater. 61 (13) (2013) 4887–4897.
[3] O.N. Senkov, G.B. Wilks, D.B. Miracle, C.P. Chuang, P.K. Liaw, Refractory high-entropy alloys, Intermetallics 18 (9) (2010) 1758–1765.
[4] O.N. Senkov, G.B. Wilks, J.M. Scott, D.B. Miracle, Mechanical properties of $Nb_{25}Mo_{25}Ta_{25}W_{25}$ and $V_{20}Nb_{20}Mo_{20}Ta_{20}W_{20}$ refractory high entropy alloys, Intermetallics 19 (5) (2011) 698–706.
[5] O.N. Senkov, D.B. Miracle, K.J. Chaput, J.P. Couzinie, Development and exploration of refractory high entropy alloys – a review, J. Mater. Res. 33 (19) (2018) 3092–3128.
[6] S. Sheikh, M.K. Bijaksana, A. Motallebzadeh, S. Shafeie, A. Lozinko, L. Gan, T.-K. Tsao, U. Klement, D. Canadinc, H. Murakami, et al., Accelerated oxidation in ductile refractory high-entropy alloys, Intermetallics 97 (2018) 58–66.
[7] F. Müller, B. Gorr, H.J. Christ, J. Müller, B. Butz, H. Chen, A. Kauffmann, M. Heilmaier, On the oxidation mechanism of refractory high entropy alloys, Corros. Sci. 159 (2019) 108161.
[8] T.M. Butler, K.J. Chaput, Native oxidation resistance of Al20Nb30Ta10Ti30Zr10 refractory complex concentrated alloy (RCCA), J. Alloys Compd. 787 (2019) 606–617.
[9] B. Gorr, F. Müller, M. Azim, H.J. Christ, T. Müller, H. Chen, A. Kauffmann, M. Heilmaier, High-temperature oxidation behavior of refractory high-entropy alloys: effect of alloy composition, Oxid. Met. 88 (3) (2017) 339–349.
[10] J.R. DiStefano, B.A. Pint, J.H. DeVan, Oxidation of refractory metals in air and low pressure oxygen gas, Int. J. Refract. Met. Hard Mater 18 (4–5) (2000) 237–243.
[11] J.H. Westbrook, D.L. Wood, "Pest" degradation in beryllides, silicides, aluminides, and related compounds, J. Nucl. Mater. 12 (2) (1964) 208–215.
[12] S. Sheikh, L. Gan, T.-K. Tsao, H. Murakami, S. Shafeie, S. Guo, Aluminizing for enhanced oxidation resistance of ductile refractory high-entropy alloys, Intermetallics 103 (2018) 40–51.
[13] D. Gaertner, K. Abrahams, J. Kottke, V.A. Esin, I. Steinbach, G. Wilde, S.V. Divinski, Concentration-dependent atomic mobilities in FCC CoCrFeMnNi high-entropy alloys, Acta Mater. 166 (2019) 357–370.
[14] J. Zhang, G.M. Muralikrishna, A. Asabre, Y. Kalchev, J. Müller, B. Butz, S. Hilke, H. Rösner, G. Laplanche, S.V. Divinski, et al., Tracer diffusion in the σ phase of the CoCrFeMnNi system, Acta Mater. 203 (2021) 116498.
[15] O.A. Lukianova, Z. Rao, V. Kulitckii, Z. Li, G. Wilde, S.V. Divinski, Impact of interstitial carbon on self-diffusion in CoCrFeMnNi high entropy alloys, Scr. Mater. 188 (2020) 264–268.
[16] D. Gaertner, J. Kottke, Y. Chumlyakov, F. Hergemöller, G. Wilde, S.V. Divinski, Tracer diffusion in single crystalline CoCrFeNi and CoCrFeMnNi high-entropy alloys: kinetic hints towards a low-temperature phase instability of the solid–solution? Scr. Mater. 187 (2020) 57–62.
[17] J. Kottke, D. Utt, B.M. Laurent, A. Fareed, D. Gaertner, L. Perriere, L. Rogal, A. Stukowski, K. Albe, S.V. Divinski, et al., Experimental and theoretical study of tracer diffusion in a series of $(CoCrFeMn)_{100-x}Ni_x$ alloys, Acta Mater. 194 (2020) 236–248.
[18] J. Kottke, B.M. Laurent, A. Fareed, D. Gaertner, L. Perrière, L. Rogal, S.V. Divinski, G. Wilde, Tracer diffusion in the Ni-CoCrFeMn system: transition from a dilute solid solution to a high entropy alloy, Scr. Mater. 159 (2019) 94–98.
[19] M. Vaidya, K.G. Pradeep, B.S. Murty, G. Wilde, S.V. Divinski, Bulk tracer diffusion in CoCrFeNi and CoCrFeMnNi high entropy alloys, Acta Mater. 146 (2018) 211–224.
[20] M. Vaidya, S. Trubel, B.S. Murty, G. Wilde, S.V. Divinski, Ni tracer diffusion in CoCrFeNi and CoCrFeMnNi high entropy alloys, J. Alloys Compd. 688 (2016) 994–1001.
[21] M. Glienke, M. Vaidya, K. Gururaj, L. Daum, B. Tas, L. Rogal, K.G. Pradeep, S.V. Divinski, G. Wilde, Grain boundary diffusion in CoCrFeMnNi high entropy alloy: kinetic hints towards a phase decomposition, Acta Mater. 195 (2020) 304–316.
[22] M. Vaidya, K.G. Pradeep, B.S. Murty, G. Wilde, S.V. Divinski, Radioactive isotopes reveal a non sluggish kinetics of grain boundary diffusion in high entropy alloys, Sci. Rep. 7 (1) (2017) 1–11.
[23] Y. Lei, S.P. Hu, T.L. Yang, X.G. Song, Y. Luo, G.D. Wang, Vacuum diffusion bonding of high-entropy $Al_{0.85}$CoCrFeNi alloy to TiAl intermetallic, J. Mater. Process. Technol. 278 (2020) 116455.
[24] Y.J. Du, J.T. Xiong, F. Jin, S.W. Li, L. Yuan, D. Feng, J.M. Shi, J.L. Li, Microstructure evolution and mechanical properties of diffusion bonding $Al_5(TiZrHfNb)_{95}$ refractory high entropy alloy to Ti_2AlNb alloy, Mater. Sci. Eng. A 802 (2021) 140610.
[25] Y. Peng, J. Li, J. Shi, S. Li, J. Xiong, Microstructure and mechanical properties of diffusion bonded joints of high-entropy alloy $Al_5(HfNbTiZr)_{95}$ and TC4 titanium alloy, J. Mater. Res. Technol. (2021).
[26] C. Jiang, R. Li, X. Wang, H. Shang, Y. Zhang, P.K. Liaw, Diffusion barrier performance of AlCrTaTiZr/AlCrTaTiZr-N high-entropy alloy films for Cu/Si connect system, Entropy 22 (2) (2020) 234.
[27] V.G. Khyzhniak, T.V. Loskutova, O.E. Datsyuk, I.S. Pohrebova, N.A. Kharchenko, T.P. Hovorun, A.I. Dehula, I.Y. Smokovich, Y.O. Kravchenko, High-entropy titanium-aluminum diffusion coatings on nickel alloy, High Temp. Mater. Processes 20 (3) (2016).
[28] V.M. Nadutov, V.F. Mazanko, S.Y. Makarenko, Tracer diffusion of cobalt in high-entropy alloys Al_xFeNiCoCuCr, Metallofiz. Noveishie Tekhnol. 39 (2017) 337–348.
[29] Thermo-Calc, High entropy alloys databases, 2022, https://thermocalc.com/products/databases/high-entropy-alloys/.
[30] M. Vaidya, S. Sen, X. Zhang, L. Frommeyer, L. Rogal, S. Sankaran, B. Grabowski, G. Wilde, S.V. Divinski, Phenomenon of ultra-fast tracer diffusion of Co in HCP high entropy alloys, Acta Mater. 196 (2020) 220–230.

[31] O.N. Senkov, J.M. Scott, S.V. Senkova, D.B. Miracle, C.F. Woodward, Microstructure and room temperature properties of a high-entropy TaNbHfZrTi alloy, J. Alloys Compd. 509 (20) (2011) 6043–6048.

[32] O.V. Sobol, A.A. Andreev, V.F. Gorban, N.A. Krapivka, V.A. Stolbovoi, I.V. Serdyuk, V.E. Filchikov, Reproducibility of the single-phase structural state of the multielement high-entropy Ti-V-Zr-Nb-Hf system and related superhard nitrides formed by the vacuum-arc method, Tech. Phys. Lett. 38 (7) (2012) 616–619.

[33] S. Vrtnik, P. Koželj, A. Meden, S. Maiti, W. Steurer, M. Feuerbacher, J. Dolinšek, Superconductivity in thermally annealed Ta-Nb-Hf-Zr-Ti high-entropy alloys, J. Alloys Compd. 695 (2017) 3530–3540.

[34] M. Feuerbacher, M. Heidelmann, C. Thomas, Plastic deformation properties of Zr-Nb-Ti-Ta-Hf high-entropy alloys, Philos. Mag. 95 (11) (2015) 1221–1232.

[35] O.N. Senkov, S.L. Semiatin, Microstructure and properties of a refractory high--entropy alloy after cold working, J. Alloys Compd. 649 (2015) 1110–1123.

[36] C.-M. Lin, C.-C. Juan, C.-H. Chang, C.-W. Tsai, J.W. Yeh, Effect of al addition on mechanical properties and microstructure of refractory $Al_xHfNbTaTiZr$ alloys, J. Alloys Compd. 624 (2015) 100–107.

[37] H. Song, F. Tian, D. Wang, Thermodynamic properties of refractory high entropy alloys, J. Alloys Compd. 682 (2016) 773–777.

[38] C.-C. Juan, M.-H. Tsai, C.-W. Tsai, W.-L. Hsu, C.-M. Lin, S.-K. Chen, S.-J. Lin, J.W. Yeh, Simultaneously increasing the strength and ductility of a refractory high-entropy alloy via grain refining, Mater. Lett. 184 (2016) 200–203.

[39] G. Dirras, L. Lilensten, P. Djemia, M. Laurent-Brocq, D. Tingaud, J.-P. Couzinié, L. Perrière, T. Chauveau, I. Guillot, Elastic and plastic properties of as-cast equimolar TiHfZrTaNb high-entropy alloy, Mater. Sci. Eng. A 654 (2016) 30–38.

[40] B. Schuh, B. Völker, J. Todt, N. Schell, L. Perrière, J. Li, J.P. Couzinié, A. Hohenwarter, Thermodynamic instability of a nanocrystalline, single-phase TiZrNbHfTa alloy and its impact on the mechanical properties, Acta Mater. 142 (2018) 201–212.

[41] L. Lilensten, J.-P. Couzinie, L. Perriere, A. Hocini, C. Keller, G. Dirras, I. Guillot, Study of a bcc multi-principal element alloy: tensile and simple shear properties and underlying deformation mechanisms, Acta Mater. 142 (2018) 131–141.

[42] S. Wang, M. Wu, D. Shu, G. Zhu, D. Wang, B. Sun, Mechanical instability and tensile properties of TiZrHfNbTa high entropy alloy at cryogenic temperatures, Acta Mater. 201 (2020) 517–527.

[43] N.D. Stepanov, N.Y. Yurchenko, S.V. Zherebtsov, M.A. Tikhonovsky, G.A. Salishchev, Aging behavior of the HfNbTaTiZr high entropy alloy, Mater. Lett. 211 (2018) 87–90.

[44] G. Dirras, J. Gubicza, A. Heczel, L. Lilensten, J.-P. Couzinié, L. Perrière, I. Guillot, A. Hocini, Microstructural investigation of plastically deformed $Ti_{20}Zr_{20}Hf_{20}Nb_{20}Ta_{20}$ high entropy alloy by x-ray diffraction and transmission electron microscopy, Mater. Charact. 108 (2015) 1–7.

[45] M.l. Hu, W.d. Song, D.b. Duan, Y. Wu, Dynamic behavior and microstructure characterization of TaNbHfZrTi high-entropy alloy at a wide range of strain rates and temperatures, Int. J. Mech. Sci. 182 (2020) 105738.

[46] J. Zỳka, J. Málek, Z. Pala, I. Andršová, J. Veselỳ, Structure and mechanical properties of TaNbHfZrTi high entropy alloy, in: Metal 2015 - 24th International Conference on Metallurgy and Materials, 2015, p. 1687.

[47] J. Jayaraj, C. Thinaharan, S. Ningshen, C. Mallika, U.K. Mudali, Corrosion behavior and surface film characterization of TaNbHfZrTi high entropy alloy in aggressive nitric acid medium, Intermetallics 89 (2017) 123–132.

[48] E. Fazakas, V. Zadorozhnyy, L.K. Varga, A. Inoue, D.V. Louzguine-Luzgin, F. Tian, L. Vitos, Experimental and theoretical study of $Ti_{20}Zr_{20}Hf_{20}Nb_{20}x_{20}$ (x = v or cr) refractory high-entropy alloys, Int. J. Refract. Met. Hard Mater 47 (2014) 131–138.

[49] M. Feuerbacher, T. Lienig, C. Thomas, A single-phase bcc high-entropy alloy in the refractory Zr-Nb-Ti-V-Hf system, Scr. Mater. 152 (2018) 40–43.

[50] A.D. Pogrebnjak, Structure and properties of nanostructured (Ti-Hf-Zr-V-Nb) n coatings, J. Nanomater. 2013 (2013).

[51] A.D. Pogrebnjak, I.V. Yakushchenko, A.A. Bagdasaryan, O.V. Bondar, R. Krause-Rehberg, G. Abadias, P. Chartier, K. Oyoshi, Y. Takeda, V.M. Beresnev, et al., Microstructure, physical and chemical properties of nanostructured (Ti-Hf-Zr-V-Nb) N coatings under different deposition conditions, Mater. Chem. Phys. 147 (3) (2014) 1079–1091.

[52] F.F. Komarov, A.D. Pogrebnyak, S.V. Konstantinov, Radiation resistance of high--entropy nanostructured (Ti, Hf, Zr, V, Nb) N coatings, Tech. Phys. 60 (10) (2015) 1519–1524.

[53] S. Taheriniya, F.A. Davani, S. Hilke, M. Hepp, C. Gadelmeier, M.R. Chellali, T. Boll, H. Rösner, M. Peterlechner, C. Gammer, et al., High entropy alloy nanocomposites produced by high pressure torsion, Acta Mater. (2021) 116714.

[54] S. Haas, M. Mosbacher, O.N. Senkov, M. Feuerbacher, J. Freudenberger, S. Gezgin, R. Völkl, U. Glatzel, Entropy determination of single-phase high entropy alloys with different crystal structures over a wide temperature range, Entropy 20 (9) (2018) 654.

[55] B. Sundman, B. Jansson, J.O. Andersson, The thermo-calc databank system, Calphad 9 (2) (1985) 153–190.

[56] D. McLean, Grain Boundaries in Metals, Oxford University Press, 1957.

[57] A. Paul, T. Laurila, V. Vuorinen, S.V. Divinski, Thermodynamics, Diffusion and the Kirkendall Effect in Solids, Springer Int. Publ., Switzerland, 2014.

[58] L.G. Harrison, Influence of dislocations on diffusion kinetics in solids with particular reference to the alkali halides, Trans. Faraday Soc. 57 (1961) 1191–1199.

[59] A.D.L. Claire, The analysis of grain boundary diffusion measurements, Br. J. Appl. Phys. 14 (6) (1963) 351.

[60] H. Mehrer, Diffusion in Solids. Fundamentals, Methods, Materials, Diffusion–Controlled Processes, Springer, 2007.

[61] A.R. Allnatt, T.R. Paul, I.V. Belova, G.E. Murch, A high accuracy diffusion kinetics formalism for random multicomponent alloys: application to high entropy alloys, Philos. Mag. 96 (28) (2016) 2969–2985.

[62] G. Neumann, V. Tölle, Self-diffusion in body-centred cubic metals: analysis of experimental data, Philos. Mag. A 61 (4) (1990) 563–578.

[63] H. Araki, Y. Minamino, T. Yamane, T. Nakatsuka, Y. Miyamoto, Pressure dependence of anomalous diffusion of zirconium in β-titanium, Metall. Mater. Trans. A 27 (7) (1996) 1807–1814.

[64] G. Neumann, C. Tuijn, Self-diffusion and impurity diffusion in group v metals, in: Pergamon Materials Series, vol. 14, Elsevier, 2008, pp. 215–238.

[65] C. Herzig, U. Köhler, M. Büscher, Temperature dependence of ^{44}Ti and ^{95}Zr diffusion and of ^{88}Zr/^{95}Zr isotope effect in the equiatomic BCC TiZr-alloy, in: Defect and Diffusion Forum, vol. 95, Trans Tech Publ, 1993, pp. 793–798.

[66] C. Herzig, U. Köhler, S.V. Divinski, Tracer diffusion and mechanism of non-arrhenius diffusion behavior of Zr and Nb in body-centered cubic Zr-Nb alloys, J. Appl. Phys. 85 (12) (1999) 8119–8130.

[67] P. Knorr, C. Herzig, Tracer diffusion of hafnium, niobium and zirconium in Hf–Nb alloys, J Phys. 7 (1995) 9185–9200.

[68] Q. He, Y. Ye, Y. Yang, The configurational entropy of mixing of metastable random solid solution in complex multicomponent alloys, J. Appl. Phys. 120 (15) (2016) 154902.

[69] A.R. Miedema, P.F. De Chatel, F.R. De Boer, Cohesion in alloysfundamentals of a semi-empirical model, Physica B+C 100 (1) (1980) 1–28.

[70] A. Mehta, Y. Sohn, Investigation of sluggish diffusion in FCC $Al_{0.25}CoCrFeNi$ high-entropy alloy, Mater. Res. Lett. 9 (5) (2021) 239–246.

[71] M.S. Daw, M. Chandross, Sluggish diffusion in random equimolar FCC alloys, Phys. Rev. Mater. 5 (4) (2021) 043603.

[72] W. Petry, A. Heiming, J. Trampenau, M. Alba, C. Herzig, H.R. Schober, G. Vogl, Phonon dispersion of the bcc phase of group-IV metals. I. bcc titanium, Phys. Rev. B 43 (1991) 10933–10947.

[73] A. Heiming, W. Petry, J. Trampenau, M. Alba, C. Herzig, H.R. Schober, G. Vogl, Phonon dispersion of the bcc phase of group-IV metals. II. bcc zirconium, a model case of dynamical precursors of martensitic transitions, Phys. Rev. B 43 (1991) 10948–10962.

[74] J. Trampenau, A. Heiming, W. Petry, M. Alba, C. Herzig, W. Miekeley, H.R. Schober, Phonon dispersion of the bcc phase of group-IV metals. III. bcc hafnium, Phys. Rev. B 43 (1991) 10963–10969.

[75] A. Glensk, B. Grabowski, T. Hickel, J. Neugebauer, Breakdown of the arrhenius law in describing vacancy formation energies: the importance of local anharmonicity revealed by ab initio thermodynamics, Phys. Rev. X 4 (2014) 011018.

[76] Y. Gong, B. Grabowski, A. Glensk, F. Körmann, J. Neugebauer, R.C. Reed, Temperature dependence of the Gibbs energy of vacancy formation of fcc Ni, Phys. Rev. B 97 (2018) 214106.

[77] X. Zhang, B. Grabowski, T. Hickel, J. Neugebauer, Calculating free energies of point defects from ab initio, Comput. Mater. Sci 148 (2018) 249–259.

[78] F. Körmann, Y. Ikeda, B. Grabowski, M. Sluiter, Phonon broadening in high entropy alloys, npj Comput. Mater. 3 (2017) 36.

[79] Y. Ikeda, B. Grabowski, F. Körmann, Ab initio phase stabilities and mechanical properties of multicomponent alloys: a comprehensive review for high entropy alloys and compositionally complex alloys, Mater Charact. 147 (2019) 464–511.

[80] X. Zhang, M.H.F. Sluiter, Ab initio prediction of vacancy properties in concentrated alloys: the case of fcc Cu-Ni, Phys. Rev. B 91 (2015) 174107.

[81] X. Zhang, S.V. Divinski, B. Grabowski, Ab initio prediction of vacancy energetics in HCP Al-Hf-Sc-Ti-Zr high entropy alloys and the subsystems, Acta Mater. 227 (2022) 117677.